Microchimica Acta (2020) 187: 296
https://doi.org/10.1007/s00604-020-04281-z

ORIGINAL PAPER

Class-selective voltammetric determination of hydroxycinnamic acids structural analogs using a WS_2/catechin-capped AuNPs/carbon black–based nanocomposite sensor

Flavio Della Pelle[1] · Daniel Rojas[1,2] · Filippo Silveri[1] · Giovanni Ferraro[3] · Emiliano Fratini[3] · Annalisa Scroccarello[1] · Alberto Escarpa[2,4] · Dario Compagnone[1]

Received: 1 February 2020 / Accepted: 13 April 2020 / Published online: 28 April 2020

Abstract

A high-performance screen-printed electrode (SPE) based nanocomposite sensor integrating tungsten disulfide (WS_2) flakes decorated with catechin-capped gold nanoparticles (AuNP-CT) and carbon black (CB) has been developed. The excellent antifouling properties of WS_2 decorated with AuNP-CT into a high conductivity network of CB results in high selectivity, sensitivity, and reproducibility for the simultaneous determination of hydroxycinnamic acid (hCN) structural analogs: caffeic (CF), sinapic (SP), and *p*-coumaric acids (CM). Using differential pulse voltammetry (DPV), the target hCNs resulted in three well-resolved oxidation peaks at SPE-CB-WS_2/AuNP-CT sensor. Excellent antifouling performance (RSD $i_{p,a} \leq 3\%$, $n = 15$ for three analytes' simultaneous measure) and low detection limits (CF 0.10 μmol L^{-1}; SP, 0.40 μmol L^{-1}; CM, 0.40 μmol L^{-1}) are obtained despite the analyzed compounds having a high passivation tendency towards carbon-based sensors. The SPE-CB-WS_2/AuNP-CT sensor was successfully applied to determine CF, SP, and CM in food samples with good precision (RSD ≤ 4%, $n = 3$) and recoveries (86–109%; RSD ≤ 5%, $n = 3$). The proposed sensor is the first example exploiting the simultaneous determination of these compounds in food samples. Given its excellent electrochemical performance, low cost, disposability, and ease of use, this SPE-CB-WS_2/AuNP-CT nanocomposite sensor represents a powerful candidate for the realization of electrochemical devices for the determination of (bio)compounds with high passivation tendency.

Keywords Transition metal dichalcogenide · Tungsten disulphide · Gold nanoparticles · Antifouling · Carbon black · Polyphenols, food analysis

Electronic supplementary material The online version of this article (https://doi.org/10.1007/s00604-020-04281-z) contains supplementary material, which is available to authorized users.

✉ Alberto Escarpa
alberto.escarpa@uah.es

✉ Dario Compagnone
dcompagnone@unite.it

[1] Faculty of Bioscience and Technology for Food Agriculture and Environment, University of Teramo, 64100 Teramo, Italy

[2] Department of Analytical Chemistry, Physical Chemistry and Chemical Engineering, Faculty of Sciences University of Alcalá, E-28871 Alcalá de Henares, Madrid, Spain

[3] Department of Chemistry "Ugo Schiff" and CSGI, University of Florence, Via della Lastruccia 3-Sesto Fiorentino, I-50019 Florence, Italy

[4] Chemical Research Institute "Andres M. del Rio", University of Alcalá, E-28871 Madrid, Spain

Introduction

Polyphenols (PCs) are secondary metabolites present in vegetables and fruits and derived foodstuff [1, 2]. They are a heterogeneous class of compounds, with important in vitro and in vivo activity [3, 4], play a role in food manufacturing and conservation (markers of quality, process, and shelf-life, sensory perception, etc.), and represent an added value for marketing (e.g., functional foods, superfoods) [1, 2]. Among PCs, hydroxycinnamic acids (hCNs) are structural and functional constituents of plant cell walls. Their hydrogen- and electron-donating abilities, as well as capacity to delocalize/stabilize phenoxyl radicals within their structure, are closely dependent on the chemical structure and, in particular, the hydroxyl function(s) arrangement [5]. The scientific community is still working to develop easy and rapid methodologies for the quali-quantitative determination and evaluation of the

reactivity of PCs. However, because of the complexity of this matter, the polyphenol analysis still lacks official methods to rely on [2].

After the boost of graphene in the analytical and materials sciences, more recently, other two-dimensional graphene-like NMs started to be studied. In particular, transitions metal dichalcogenides (TMDs) have received great attention because of their chemistry, physical properties, and versatility [6–10]. However, their employment in the development of sensors for the analysis of real matrices needs to be further explored [7, 11]. The main limitation of TMDs [9] is linked to both the intrinsic low conductivity and massive tendency to the "restacking" phenomenon, regardless of the type of synthesis/exfoliation and the resulting conformation of the sheets [12]. Nevertheless, TMDs have demonstrated to be elective building blocks for the development of hybrids nanomaterials, giving rise to improved and sometimes unexpected properties [8–11]. However, despite metal nanostructure-decorated MoS_2 nanocomposites having been extensively studied [8], the use of WS_2 has been little explored [12, 13] particularly in the sensor's field [14].

The simultaneous determination of different PCs in food has been attempted using different nanocomposite-based sensors [15–17], commonly using a pre-concentration step (accumulation). In this regard, Puangjan et al. [15] reported on a PCs/ZrO_2/Co_3O_4/reduced graphene oxide composite electrode to detect gallic, caffeic, and protocatechuic acids in food samples, while multi-walled carbon nanotubes functionalized with AuNP-CT and p-aminothiophenol were used by Yola et al. [16] to assess quercetin and rutin content in fruit juices. Elçin et al. have exploited a ruthenium nanoparticle anchored calix[4]amidocrown-5 functionalized reduced graphene oxide electrode to simultaneously analyze quercetin, morin, and rutin in grape wine [17]. TMDs have been little explored in food polyphenols sensing [9, 10]. Our group has demonstrated that MoS_2 exhibits antifouling properties towards polyphenols detection, and, coupled with highly conductive CB, improves the electrochemical sensing of olive oil ortho-diphenols [10] and cocoa catechins [9]. Moreover, this antifouling ability has been recently confirmed in a comprehensive study, where TMDs (MoS_2, $MoSe_2$, WS_2, and WSe_2) demonstrated better electrochemical performance and enhanced antifouling properties, towards flavonoid's oxidation, compared with carbon-based electrodes [18].

The aim of this work has been to develop a hybrid WS_2-based electrochemical sensor for the simultaneous analysis of hCNs as non-flavonoid phenols. For this kind of compounds, the redox potentials and the relative contents can be considered a good measure of antioxidant activity [5]. Indeed, the electrochemistry of hCN-based antioxidants is governed by structure-property-activity relationships. Three hCN structural analogs with different hydroxylic moieties have been selected as target compounds: caffeic acid (CF), sinapic acid (SP), and p-coumaric acid (CM). To the best of our knowledge, there are no reports about the simultaneous determination of these compounds in the literature, despite they are commonly found in food. This can be probably attributed to the following: (i) the strong passivating tendency of hCNs towards carbon-based sensors [2], (ii) the poor electroactivity of SP and CM [19, 20], and (iii) the hCNs very similar structure that makes voltammetric discrimination/differentiation challenging. The SPE-CB-WS_2/AuNP-CT sensor developed here takes advantage of the combination of green-synthesized catechin-based gold nanoparticles coupled with WS_2 nanoflakes onto a highly electroactive CB network.

Materials and methods

Reagents, stock solutions, and samples

Caffeic, sinapic, and *p*-coumaric acids were purchased from Sigma-Aldrich (St Louis, MO, USA). Potassium ferrocyanide, potassium ferricyanide, potassium chloride, sodium phosphate monobasic monohydrate ($NaH_2PO_4 \cdot H_2O$), sodium phosphate dibasic anhydrous (Na_2HPO_4), sodium citrate, sodium borohydride, N-N-dimethylformamide (DMF), methanol, cetyltrimethylammonium chloride (CTAC 25.0% in water), hydrogen tetrachloroaurate ($HAuCl_4 \cdot 3H_2O$, 99.9%), fructose, glucose, sucrose, citric acid, acetic acid, malic acid, succinic acid, tartaric acid, oxalic acid, quinic acid, and shikimic acid were purchased from Sigma-Aldrich (St Louis, MO, USA). Carbon black N220 was obtained from Cabot Corporation (Ravenna, Italy). WS_2 (99.8%, metals basis) was purchased from Alfa Aesar (Ward Hill, MA). Polyphenol standard's stock solutions were prepared in methanol at a concentration of 1.0×10^{-2} mol L^{-1} and stored at − 18 °C in the dark. Milli-Q water (18.2 MΩ) was used for all the experiments. Rapeseed oil, apple puree, apple homogenized, and apple juice were purchased from a local market. *Kalanchoe crenata* lyophilized leaves were purchased from a local market in Burundi.

Apparatus

Cyclic voltammetry (CV), differential pulse voltammetry (DPV), and electrochemical impedance spectroscopy (EIS) measures were performed by using a portable Palmsens 4 Potentiostat/Galvanostat/Impedance Analyzer (Palm Instruments BV, Houten, Netherlands) equipped with PS trace software. Screen-printed electrodes (SPEs) with a three-electrode configuration (working and counter electrodes of graphite, and silver as pseudo-reference electrode) from EcoBioServices (Florence, Italy) were used. Absorbance measurements were obtained using a JENWAY 6400 Spectrophotometer from Barloworld Scientific (Staffordshire,

UK). Scanning electron microscopy (SEM) and energy-dispersive X-ray spectroscopy (EDX) were performed with a ΣIGMA high-resolution scanning electron microscope (Carl Zeiss Microscopy GmbH, Germany).

CB-WS_2/AuNP-CT nanocomposite formation and electrode modification

Preparation of catechin-capped gold nanoparticles (AuNP-CT)

The AuNP-CT synthesis was carried out according to Della Pelle et al. [19, 20] with some modifications (Scheme S1). The reaction mix containing 20 μL of CTAC (25.0% in water), 50 μL of $HAuCl_4$ (20 mmol L^{-1}), and 100 μL of catechin (1 mmol L^{-1}) was prepared in 0.1mol L^{-1} phosphate buffer (PB) at pH 8 in a final volume of 1 mL. The mixture was orbitally stirred (at 300 rpm) for 2 min, treated with a hot bath at 45 °C for 10 min, and then placed in ice overnight to achieve the AuNP-CT precipitation (precipitated nanoparticles can be stored for 15 days at + 4 °C). Afterward, the supernatant was removed and the nanoparticles were recovered in 1 mL of H_2O. The absorbance of the obtained AuNP-CT was centered at 540 nm (LSPR maximum), and absorbance values between 2.0 ± 0.1 accepted.

WS_2 decoration with AuNP-CT (WS_2/AuNP-CT)

Then, 2 mg mL^{-1} WS_2 dispersion was prepared in DMF, vortexed for 2 min, and treated with an ultrasonic bath (3000683 Ultrasons Selecta, Barcelona, Spain) for 5 h at low temperature (15 °C). Afterward, the coarser part of the material was removed by centrifugation (300*g*, 0.5 h). Then, 200 μL of WS_2 was mixed with 800 μL of AuNP-CT in the ultrasonic bath for 1 h at room temperature (mixing each 20 min) and left to interact at 4 °C overnight. The obtained WS_2 flakes decorated with AuNP-CT were centrifuged (700*g*, 5 min), and the pellet was resuspended in 200 μL of DMF (see Scheme S1).

Preparation of the CB-WS_2/AuNP-CT sensor

The WS_2/AuNP-CT was mixed with 200 μL of 1 mg mL^{-1} CB dispersion (previously prepared by 1 h of sonication in DMF:H_2O 1:1 according to Della Pelle et al. [9, 21]). The SPE electrodes were modified via drop-casting of 6 μL of the nanohybrid suspension (by three different depositions of 2 μL, each deposition preceded by 1 min of sonication).

Microscopic and elemental analysis

Field emission scanning electron microscopy (FE-SEM) coupled with energy-dispersive X-ray spectroscopy (EDX) was performed with a ΣIGMA high-resolution scanning electron microscope (Carl Zeiss Microscopy GmbH, Germany). The electrodes' morphological characterization was assessed on the uncoated working electrode surface, using an acceleration potential of 2 kV at a working distance of about 4 mm. Energy-dispersive X-ray analysis (EDX) was performed using a silicon drift detector (Oxford Instruments) coupled with SEM using a working distance of about 8.5 mm and an accelerating potential of 15 kV, analyzing a sampling area ranging from 0.06 to 0.09 mm^2.

Electrochemical measurements

All the materials and the obtained nanocomposites were investigated by cyclic voltammetry (CV) and electrochemical impedance spectroscopy (EIS) using a solution of 1 mmol L^{-1} $[Fe(CN)_6]^{3-/4-}$ and 0.1 mol L^{-1} KCl. CV was performed at a scan rate of 50 mV s^{-1}. EIS experiment was achieved using a sinusoidal wave of 5 mV amplitude in the 10^5 to 10^{-1} Hz frequency range, setting the potential at open circuit. Nyquist plots were fitted using the Randles modified equivalent circuit. CV and DPV were also employed to assess the electrochemical response of the sensors to the analytes (CF, SP, and CM). The measurements were carried out by depositing 100 μL of the analyte solution onto the working electrode surface. CVs of polyphenols was performed with a scan rate of 50 mV s^{-1}, in a potential window from − 0.2 V to 0.8 V (vs. pseudo Ag/AgCl). DPVs of the analytes were performed individually and in mixture and the parameters were optimized to improve the sensitivity and the resolution (potential range between − 0.1 V and 0.65 V, pulse width 50 ms, modulation amplitude 50 mV, scan rate of 25 mV s^{-1}).

Samples' preparation and analysis

Different samples were employed to prove the potential usability of the proposed sensor. The rapeseed oil extraction was performed according to Pirisi et al. [22], with some modifications. Six grams of rapeseed oil was dissolved in 3 mL of hexane and 6 mL of MeOH:H_2O solution (60:40 v/v); then, the sample was stirred for 1 min (with vortex) and centrifuged for 5 min at 3000 rpm. Thus, the polar fraction was collected and the extraction procedure was repeated two times. Finally, the extract was washed with 6 mL of hexane, and after centrifugation (3000 rpm, 5 min), the polar fraction was separated and dried by using a rotavapor. The "dried" polar fraction was recovered with 1.5 mL of MeOH:H_2O solution (60:40 v/v) and stored at − 20 °C in the dark. One gram of the apple puree, 1.0 g of apple homogenized, 0.15 g of lyophilized kalanchoe, and 2.0 g of apple juice were dissolved in a MeOH:H_2O solution (80:20 v/v) with a ratio of 1:5, 1:5, 1:33, and 1:2, respectively. The samples were treated with an ultrasonic bath for 5 min and stirred with an orbital shaker at 300 rpm, 30 min in the dark at room temperature. Afterward, the samples were

centrifuged (700*g*, 5 min) and the supernatant was recovered and adjusted to the respective starting volume with MeOH:H_2O solution (80:20 v/v) and stored at − 20 °C in the dark. The electrochemical measurements on the extracts were carried out using DPV ("Electrochemical measurements"). Before analysis, the samples were diluted in 0.01 mol L^{-1} (pH 7.0) phosphate buffer (to fit the calibration linear range) at the following ratios: 1:250 rapeseed oil, apple puree, apple homogenized; 1:25 apple juice; 1:400 *Kalanchoe crenata*. As the polyphenols in samples are present in different ratios [23], the analysis of the samples has been conducted using the standard addition method. All samples were analyzed in triplicate.

Results and discussion

Sensor design

In order to develop an electrochemical sensor able to selectively measure hCNs and similar structural analogs with same hydroxyl moieties' configuration in the phenolic structure, a pertinent nanomaterial-based configuration was employed. Scheme 1 illustrates the SPE-CB-WS_2/AuNP-CT sensor architecture (described in detail in "CB-WS_2/AuNP-CT nanocomposite formation and electrode modification").

WS_2 flakes' decoration with AuNP-CT was carried out using a sonochemical strategy to obtain a WS_2/AuNP-CT antifouling/conductive nanohybrid (Scheme 1A). During WS_2/AuNP-CT decoration, the AuNP-CT solution (Fig. S1, red line) resulted completely decolored (no LSPR signal indicating that AuNP-CT were adsorbed on WS_2 flakes), and a well-deposited gray/rubin-red pellet (formed by WS_2/AuNP-CT) was obtained (see Scheme S1). The latter, after resuspension, gives a colloidal dispersion with an LSPR maximum at 540 ± 7 nm (Fig. S1, blue line), definitely indicating the presence of the two nanomaterials. Finally, the decorated WS_2/AuNP-CT were assembled into a highly electroactive CB network (Scheme 1B) to form the final nanocomposite (Scheme 1C), which was employed to modify the SPEs (Scheme 1D) giving rise to the SPE-CB-WS_2/AuNP-CT electrochemical sensor.

Despite that the decoration of non-graphene "layered" nanomaterials (e.g., MoS_2, $HxTiS_2$) with AuNPs has been attempted using different strategies (auto assembling exploiting gold thiophilicity, electrodeposition, etc.) [8, 24, 25], the decoration of WS_2 with AuNPs has been explored in lesser extension [12, 13] particularly for the development of sensors [14]. In this work, the WS_2 decoration was attempted using AuNPs synthesized using catechin (AuNPs-CT), sodium citrate, and sodium borohydride as mild reducing agent following the strategy of "WS_2 decoration with AuNP-

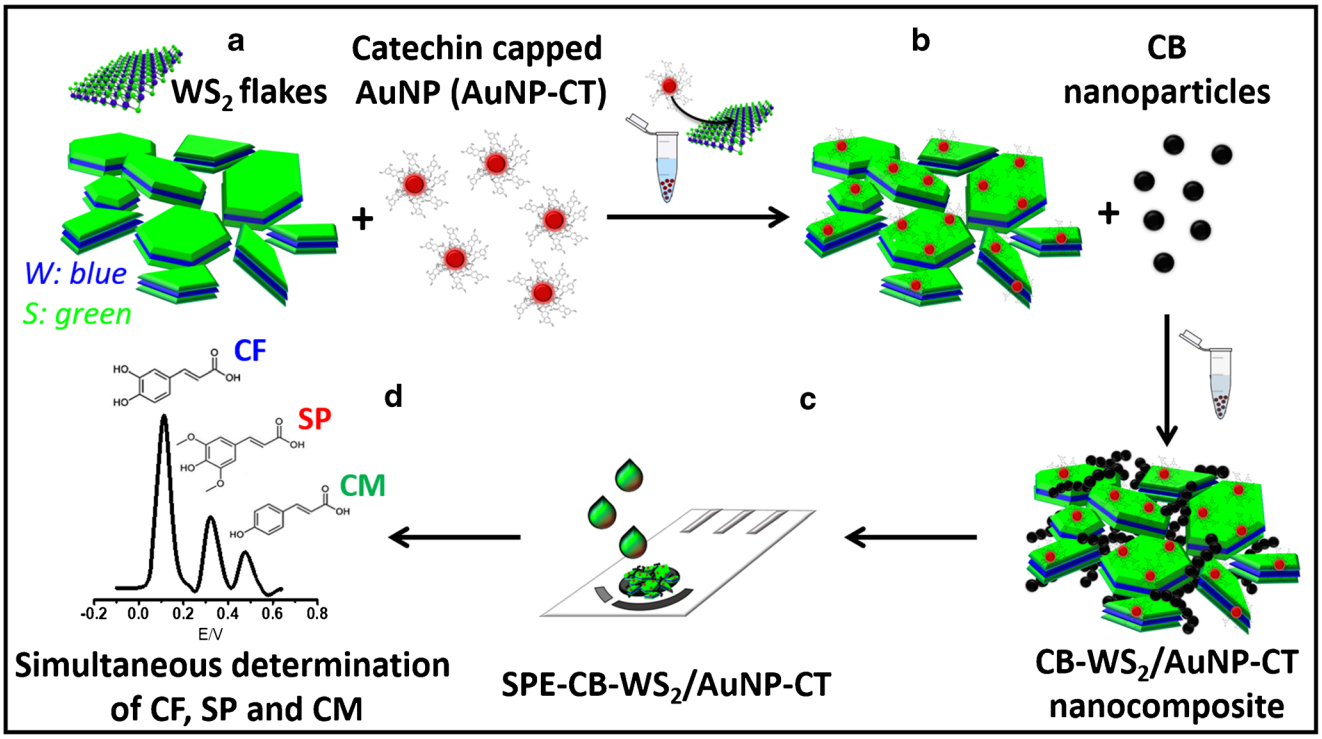

Scheme 1 Scheme of the SPE-CB-WS_2/AuNP-CT architecture for hydroxycinnamic acid structural analogs electrochemical sensing. (**A**) WS_2 decoration with AuNP-CT (a detailed scheme of this step is depicted in Scheme S1). (**B**) Assembly of WS_2/AuNP-CT into CB. (**C**) SPE modification with the CB-WS_2/AuNP-CT nanocomposite. (**D**) DPV simultaneous determination of CF, SP, and CM

CT (WS_2/AuNP-CT)" section (schematized in Scheme S1). Only AuNP-CT with their peculiar colloidal chemistry allowed an effective WS_2 nanoflakes' decoration. The AuNP-CT assembly in the WS_2 "sheets" resulted in an enhanced conductivity with retention of antifouling properties due to WS_2. On the other hand, both sodium citrate and sodium borohydride synthesized AuNPs failed to decorate the WS_2 flakes; this was evident by the persistence of the ruby-red color, during the decoration process, indicating the failed interaction and the persistence of AuNPs in solution. This evidence points out the key role of the AuNP-CT colloidal chemistry, which allows a strong interaction with the WS_2 nanoflakes in the experimental conditions used. This behavior is probably related to the "catechins" (catechins reacted/partially reacted/polymerized) shell around the gold metal core [19, 20, 26], which allows high dispersibility in water even in the presence of DMF, and probably a lower repulsion towards the WS_2 surface.

Morphological and electrochemical characterization

Figure 1 reports SEM micrographs (A–C) acquired at different magnifications on the SPE-CB WS_2/AuNP-CT electrode, and EDX analysis (D).

Figure 1 A depicts the uniform distribution of all the nanocomposite components and the total coverage of the electrode surface. Looking at micrographs with higher magnification (Fig. 1B), it is possible to evidence the presence of WS_2 flakes with a broad size distribution centered at around 800 nm (mean size calculated on more than 100 WS_2 flakes). CB primary particles are also visible in Fig. 1B, revealing the co-presence of the components and their "interaction" while their pristine morphology is fully retained. This behavior can be attributed to the flake-like conformation of WS_2 that favors their floating to the surface [9, 10]. The presence of AuNP-CT with a size distribution centered at around 5 ± 1 nm (particle size distribution in Fig. S3B calculated on 200 AuNP-CT, using 300 kX magnifications SEM images) is further assessed by the micrograph at higher magnification (300 kX) in Fig. 1C and confirmed by EDX analysis (Fig. 1D), where the amount of Au with respect to W was found around 0.4:1.0. Additional SEM micrographs are reported in Fig. S2 to better visualize the morphology of the obtained electrodes. The catechin ability to give rise to AuNPs stabilized by the same "reacted-catechin" (localized in the AuNPs shells) has been proved [19, 20, 26], and the formation of a "catechins" layer on the surface of gold nanoparticles demonstrated by Raman spectroscopy [27] and microscopic (TEM) analysis [28]. In addition, the ability of tea catechins to interact with the WS_2 in solution, during the exfoliation phase, has been reported as well [29]. In this study, catechins acting as surfactants demonstrated to assist the sonication-assisted aqueous exfoliation of TMDs enhancing the TMD sheets' water dispersibility.

On the other hand, the electrochemical behavior of the modified electrodes was investigated by cyclic voltammetry (CV). Figure 2 A shows CVs of 1 mmol L^{-1} $[Fe(CN)_6]^{3-/4-}$ at bare SPE, SPE-WS_2, SPE-CB, SPE-WS_2/AuNP-CT, SPE-CB-WS_2, and SPE-CB-WS_2/AuNP-CT. To better understand the

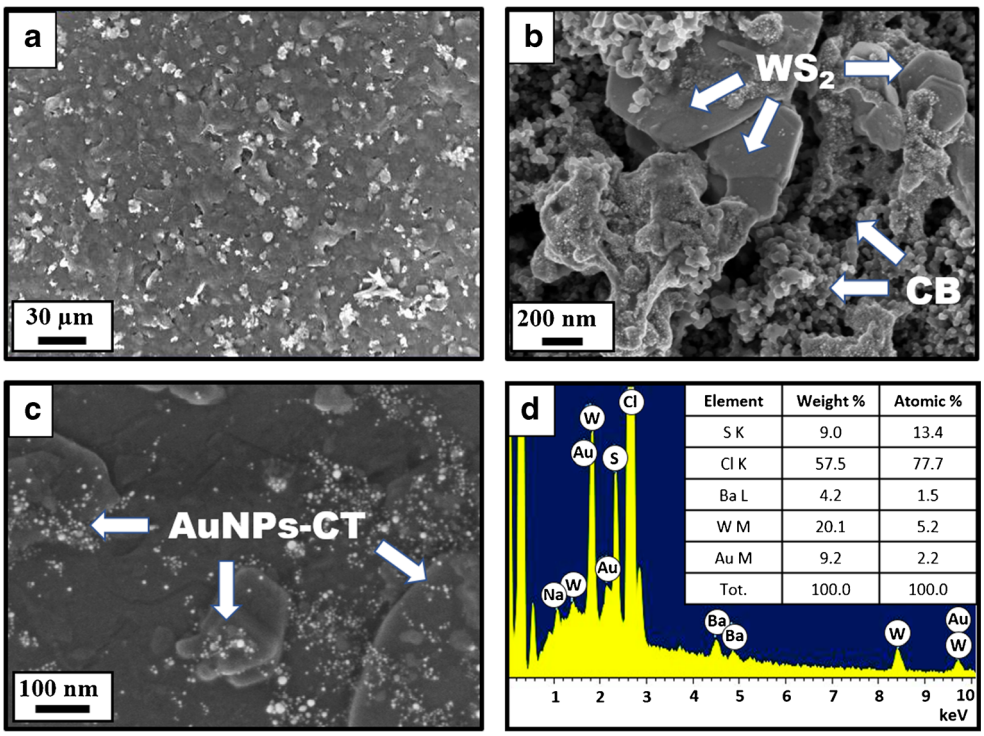

Fig. 1 SEM at different magnifications of the SPE-CB-WS_2/AuNP-CT: 1 kX (**A**), 100 kX (**B**), 300 kX (**C**). EDX spectrum from SPE-CB-WS_2/AuNP-CT (**D**)

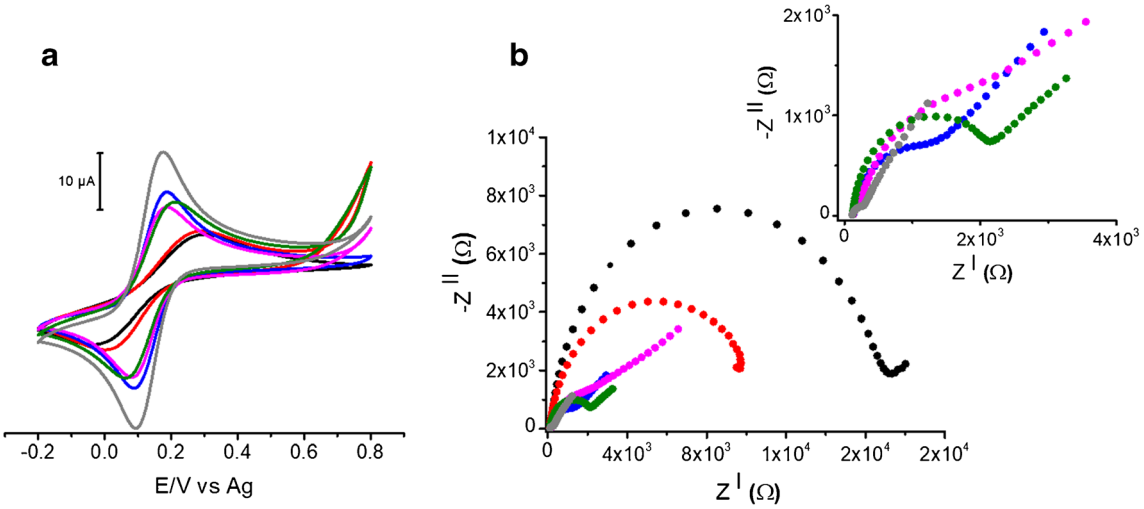

Fig. 2 Electrochemical characterization of the set of electrodes: (**A**) cyclic voltammograms at 50 mV s^{-1} and (**B**) electrochemical impedance spectra (inset reports the Nyquist plot magnification at low frequencies region). Conditions: 1 mmol L^{-1} $[Fe(CN)_6]^{3-/4-}$ redox probe in 0.1 mol L^{-1} KCl (pH 7.0). The code color–based legend is as follows: bare SPE (black), SPE-WS_2 (red), SPE-CB (blue), SPE-WS_2/AuNP-CT (violet), SPE-CB-WS_2 (green), and SPE-CB-WS_2/AuNP-CT (gray)

contribution of each component in the final nanocomposite, the heterogeneous rate constant (k^0) was calculated using the Nicholson method (for details, see ESM 2, Fig. S4) [30, 31]. The obtained electrochemical features are listed in Table S1.

Figure 2 A (see also Table S1) indicates higher electrocatalytic activity with faster electron transfer (highest k^0) kinetics for the SPE-CB-WS_2/AuNP-CT. In particular, k^0 values follow this trend: SPE < SPE-WS_2 < SPE-CB-WS_2 < SPE-WS_2/AuNP-CT < SPE-CB < SPE-CB-WS_2/AuNP-CT, clearly indicating the contribution of both CB and AuNP-CT in the improvement of the final nanocomposite performance. In order to prove the enhanced properties of WS_2 decoration with AuNP-CT following the proposed sonochemical strategy, the WS_2 decoration has also been attempted via direct drop-casting of AuNP-CT. Nevertheless, worse electrochemical performances were obtained (see Table S2).

Then, EIS was employed to further characterize the interfacial properties of the whole set of electrodes(Fig. 2B). The data have been fitted considering the Randles equivalent circuit . As expected, the higher charge transfer resistance (R_{ct}) was obtained with the bare SPE ($R_{ct} = 1.6 \times 10^4$ Ω), followed by the SPE-WS_2 ($R_{ct} = 9.2 \times 10^3$ Ω). The latter little R_{ct} decrease has been already reported for TMD-modified SPEs, in which TMDs acts as a semi-conductor not allowing strong R_{ct} decrease [7, 8], while R_{ct} values of 2.3×10^3, 2.1×10^3, 9.8×10^2, and 2.8×10^2 Ω were obtained with the SPE-CB-WS_2, SPE-WS_2/AuNP-CT, SPE-CB, and SPE-CB-WS_2/AuNP-CT, respectively. Interestingly, the final nanocomposite (CB-WS_2/AuNP-CT) significantly decreases R_{ct} even in comparison with CB-based electrodes, which are highly conductive transducers [32 35].

Therefore, the AuNP-CT decoration significantly improves the electrochemical performances of WS_2, and the combination of AuNP-CT and CB results in a synergistic effect that further promotes $[Fe(CN)_6]^{3-/4-}$ electron transfer.

Electrochemical behavior of cinnamic acid hydroxy-derivatives

Figure 3 A–C reports the cyclic voltammograms obtained for the target hCNs, while Fig. 3 D shows the differential pulse voltammograms of a mixture containing CF, SP, and CM.

The CV anodic peaks obtained at SPE-CB-WS_2/AuNP-CT are significantly higher than those obtained at bare SPE for all hCNs, in particular, 20-, 13-, and 25-fold for the CF, SP, and CM, respectively. In all cases, the oxidation potential is lower ($E_{p,a}$: CF 127 mV, SP 340 mV, and CM 491 mV) with respect to the bare SPE ($E_{p,a}$: CF 244 mV, SP 380 mV, and CM 540 mV), revealing an electrocatalytic effect for hCN detection.

CF reversibility improves using the SPE-CB-WS_2/AuNP-CT (ΔE 68 mV vs. ΔE 220 mV of the bare SPE) in comparison with the individual nanomaterial-modified electrodes. Noteworthy, the WS_2 itself (SPE-WS_2) gives rise to significantly higher oxidation peaks, compared with the bare electrode (SPE), in particular for the poorly reversible analytes SP and CM. This behavior indicates a capacity of the WS_2 to interact with the target hCNs. However, WS_2 by itself returns broadened and little defined peaks, while more defined and higher oxidation peaks, occurring at lower potentials, can be detected for the hybrid CB-WS_2 sensor. This improvement is more pronounced in the presence of AuNP-CT (SPE-CB-

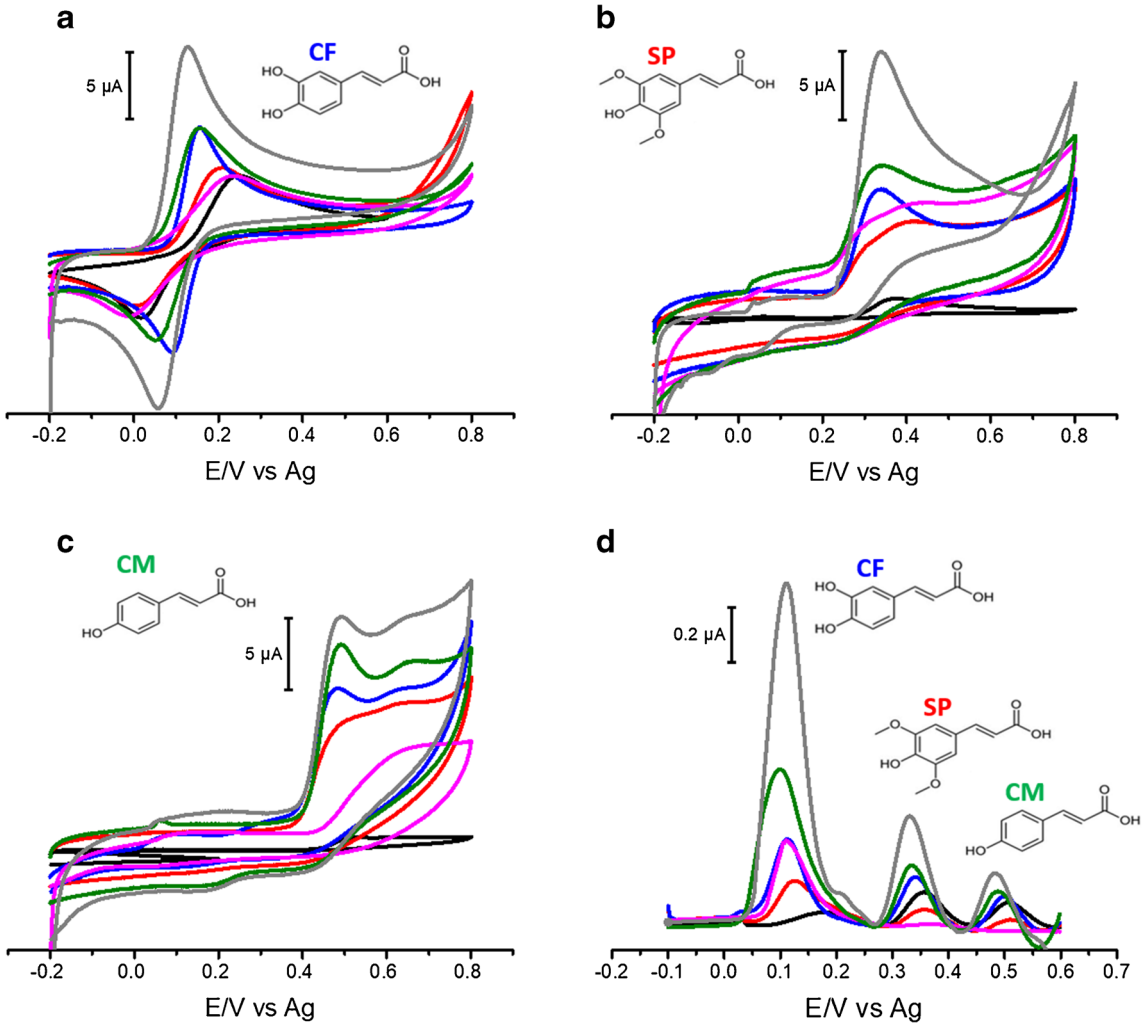

Fig. 3 Cyclic voltammograms at 50 mV s^{-1} of 0.1 mmol L^{-1} CF (**A**), 0.2 mmol L^{-1} SP (**B**), and 0.2 mmol L^{-1} CM (**C**) in 0.1 mmol L^{-1} PB + 0.1 KCl (pH 7.0) at the set of modified electrodes. (**D**) Differential pulse voltammograms (pulse width 50 ms, modulation amplitude 50 mV, scan rate of 25 mV s^{-1}) of a mixture containing CF, SP, and CM 20 μmol L^{-1} each in 0.1 mmol L^{-1} PB + 0.1 KCl (pH 7.0) at the set of modified electrodes. The code color–based legend is as follows: bare SPE (black line), SPE-WS_2 (red line), SPE-CB (blue line), SPE-WS_2/AuNP-CT (violet line), SPE-CB-WS_2 (green line), and SPE-CB-WS_2/AuNP-CT (gray line)

WS_2/AuNP-CT), because of the higher conductivity of the hybrid nanocomposite.

The electrochemical behavior of the whole set of electrodes was also evaluated after consecutive CVs ($n = 5$) in the presence of 0.1 mmol L^{-1} CF, and 0.2 mmol L^{-1} SP and CM. The voltammetric current retention (calculated comparing the first and the last scans) resulted to be ≥ 9% for SPE, ≥ 95% for SPE-WS_2, ≥ 49% in the case of SPE-CB, ≥ 93% for SPE-WS_2/AuNP-CT, ≥ 91% for SPE-CB-WS_2, and ≥ 94% for SPE-CB-WS_2/AuNP-CT. These data indicate the WS_2 ability to decrease permanent fouling of the sensor. Interestingly, this feature was also observed with monophenolic compounds (SP and CM), classically characterized by a very strong passivating tendency on carbon electrodes [2].

Figure 3 D reports the DPVs of a mixture of CF, SP, and CM obtained using bare SPE, SPE-WS_2, SPE-CB, SPE-WS_2/AuNP-CT, SPE-CB-WS_2, and SPE-CB-WS_2/AuNP-CT. The SPE-CB-WS_2/AuNP-CT exhibits three sharp peaks at 110 mV, 330 mV, and 490 mV for CF, SP, and CM, respectively. Using the SPE-CB-WS_2/AuNP-CT, an impressive current intensity was obtained for CF, 24.0-fold higher than the bare electrode, 3.5-fold higher than SPE-CB, and 2.0-fold higher than SPE-CB/WS_2. Moreover, clear improvements were obtained even for SP (3.4-fold SPE, 2.3-fold SPE-CB, 1.8-fold SPE-CB/WS_2) and CM (3.0-fold SPE, 2.2-fold SPE-CB, 1.5-fold SPE-CB/WS_2).

These data demonstrate the synergistic effect of the CB-WS_2/AuNP-CT nanocomposite (in terms of selectivity, sensitivity, and fouling resistance) proving its capability for the

simultaneous detection of CF, SP, and CM. As it was stated in the "Introduction" section, the voltammetric simultaneous determination of CF, SP, and CM has been not reported in the literature and their determination is classically obtained with separative methods. Probably, this lack of electrochemical methods is related to the hCN high passivating tendency.

Analytical performance of the SPE-CB-WS_2/AuNP-CT electrochemical sensor

Figure 4 illustrates the simultaneous calibration voltammograms for the target hCNs obtained using the SPE-CB-WS_2/AuNP-CT.

Table 1 lists the obtained analytical features. Very good linear concentration ranges and suitable LODs were obtained for the three hCNs. Noteworthy, the concomitant presence of the three target hCNs had not severe influence on the whole calibration performance (the individual calibrations of the hCN target are reported in Fig. S5).

Individual and simultaneous determination of SF, SP, and CM return repeatable results (RSD $i_{p,a} \leq 3\%$, $n = 3$) and a very good inter-electrode precision (RSD $i_{p,a} \leq 4\%$, $n = 10$), indicating a reproducible and robust fabrication strategy. Long-term stability was also tested for 6 months (control every week), checking the DPV's responses of the sensor towards CF, SP, and CM assayed simultaneously. The responses of the SPE-CB/WS_2-AuNP-CT sensor slightly decrease in the first 2 months to 95% and remain stable for the following 4 months (up to 94%).

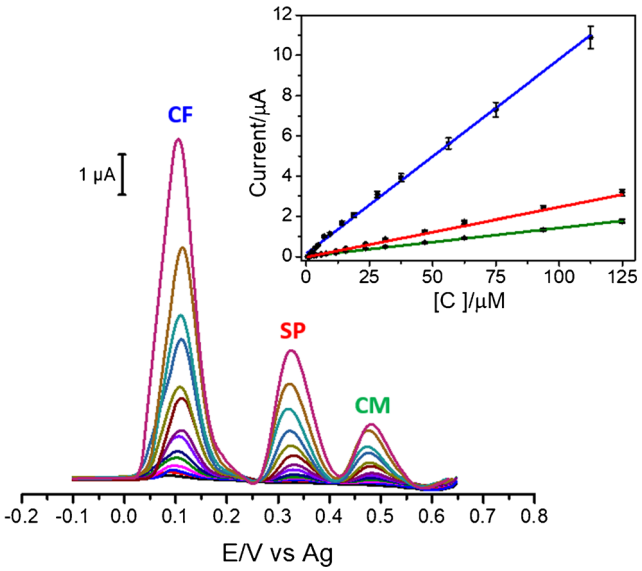

Fig. 4 Differential pulse voltammograms for the simultaneous calibration of CF (0.3–112.0 μmol L^{-1}), SP (1.2–125.0 μmol L^{-1}), and CM (1.3–125.0 μmol L^{-1}) at SPE-CB-WS_2/AuNP-CT sensor. Insets: calibration plots for CF (blue line), SP (red line), and CM (green line) ($n = 15$ assayed concentrations, $n = 3$ replicates each). Conditions: 0.1 mmol L^{-1} PB + 0.1 KCl, pH 7.0; pulse width 50 ms, modulation amplitude 50 mV, scan rate of 25 mV s^{-1}

To further prove the SPE-CB-WS_2/AuNP-CT antifouling ability even in the case of simultaneous analysis of the studied hCNs, DPVs of the ternary mixture at fixed concentrations (CF, SP, and CM 20.0 μmol L^{-1} each) have been run before and after the whole set of measurements ($n = 15$) of the calibration(Fig. S6). The signal retention obtained has been 98%, 97%, and 97% for CF, SP, and CM, respectively, confirming the electrode ability to avoid permanent passivation, commonly caused by these compounds.

Simultaneous determination of CF, SP, and CM in food samples

In order to prove the applicability of the SPE-CB-WS_2/AuNP-CT sensor, five commercial products (rapeseed oil, *Kalanchoe crenata*, apple puree, apple homogenized, and apple juice) were analyzed. Figure 5 shows the obtained voltammograms.

For the sake of clarity, we need to take into account that in nature polyphenols are never found as single compounds, but they are always present in complex mixtures in different ratios. Therefore, the DPV's signals obtained have been assigned not only to the individual hCN standard but also to the combined effect of other analogous structures (i.e. same hydroxyl moieties' arrangement in the phenol structure) potentially present in the samples. Thus, this method should be considered a class-selective index, able to return information on the polyphenols' structure and amount. In particular, with the proposed sensor an hCN-based triple index can be obtained, able to discriminate hCN with different hydroxylic functions' arrangement and therefore different antioxidant capacities. Thus, the proposed indexes' result able to simultaneously discriminate (i) CF equivalents (peak I), ortho-diphenols' structures that are oxidized at lowest oxidation potential ($E_{p,a}$ ~ 110 mV), possessing higher antioxidant capacity; (ii) SP equivalents (peak II), monophenols with a 4-hydroxy-3,5-dimethoxy structure, detected at an intermediate oxidation potential ($E_{p,a}$ 330 mV), with intermediate antioxidant capacity; and (iii) SP equivalents (peak III), monophenols, with higher oxidation potential ($E_{p,a}$ 490 mV) and lower antioxidant capacity. This index results fully consistent with the literature, where the antioxidant capacity series of PCs follows the trend o-diphenols > methoxy-substituted monophenols > monophenols [19, 20]. Thus, in this case, the oxidation potential and the peak intensity can return qualitative and quantitative information on the antioxidant capacity. For this reason, this approach may result particularly appealing for samples rich in cinnamic acids and polyphenols with similar structures but different antioxidant capacities. Therefore, as shown in Fig. 5, sample endogenous polyphenols can be classified with the proposed indexes. Table 2 lists the hCN equivalents' quantitative levels obtained for sample analysis.

As expected, among the analyzed compounds, only those having CF-like structures are found in all the samples [23],

Table 1 Calibration equations and analytical features for individual (top) and simultaneous (bottom) determination of the target hCNs at SPE-CB-WS_2/AuNP-CT

Analyte	Linear range (μmol L^{-1})	Linear equation ($y = i_{p,a}$/μA; x = [analyte]/μmol L^{-1})	R^2	LOD (μmol L^{-1})	LOQ (μmol L^{-1})
Caffeic acid[a]	0.3–200.0	$y = 0.0869x - 0.0473$	0.9998	0.1	0.3
Sinapic acid[a]	0.6–300.0	$y = 0.0309x - 0.0458$	0.9996	0.2	0.6
p-Coumaric acid[a]	0.9–175.0	$y = 0.0186x - 0.0019$	0.9990	0.3	0.9
Caffeic acid[b]	0.3–112.0	$y = 0.0945x + 0.1564$	0.9990	0.1	0.3
Sinapic acid[b]	1.2–125.0	$y = 0.0250x + 0.0198$	0.9990	0.4	1.2
p-Coumaric acid[b]	1.3–125.0	$y = 0.0141x + 0.0211$	0.9990	0.4	1.3

[a] Data obtained increasing the concentration of one analyte, keeping constant the concentrations of the other two hCNs. [b] Data obtained increasing the three analytes' concentrations simultaneously ($n = 3$)

while SP is detected only in rapeseed oil. Indeed, in the literature, it is reported that SP and compounds with SP moiety are the main phenols in rapeseed. CM is present at high concentration only in the *Kalanchoe crenata*, while it has lower concentrations compared with other endogenous polyphenols in the other samples. In all cases, the CF, SP, and CM peaks appear at potentials close to the standards with an $E_{p,a}$ standard deviation ≤ 9 mV, making the peak assignment easy and reliable. Moreover, a very good intermediate precision was obtained for all the analyzed samples (RSD ≤ 4, $n = 3$).

Recovery studies were also carried out to demonstrate the sensor's accuracy and capabilities for reliable quantitation of the hCN equivalents in food samples. Table 2 reports the recovery levels and the precision obtained with the investigated samples. The obtained values ranged from 86 to 109%, with RSD ≤ 5%, revealing an acceptable accuracy, taking into account the complexity of the samples. In addition, the spiked samples CF, SP, and CM exhibit the same $E_{p,a}$ of the standards (SD ≤ 7 mV). These data unambiguously prove that the proposed sensor is suitable for food sample's analysis.

The influence of potential interference effects caused by species commonly found in these samples was also examined. To this aim, the main ions, sugars, and organic acids were studied, choosing the concentrations of the potential interferents according to literature data [36, 37]. The tolerable signal perturbation limit has been settled at a relative peak's variation maximum of 5%. The main sugars (fructose, glucose, and sucrose) at 50-fold excess with respect to the values found in samples failed to interfere. In addition, as expected, no interference has been found using up to 200-fold excess of Na^+, K^+, Mg^{2+}, Ca^{2+}, Cl^-, and HCO_3^-. Among the organic acids, citric, acetic, malic, succinic, tartaric, oxalic, quinic, and shikimic acids, up to 100-fold, their usual concentrations failed to interfere; above these concentrations, pH changes can perturb the measurement. Ascorbic acid can potentially react with the sensor at high concentrations due to its reducing activity. Nevertheless, in the studied samples, ascorbic acid is naturally present at low levels compared with PCs. Thus, considering the sample concentrations and the dilution required to assay the samples (at least 25-fold), ascorbic acid does not interfere in the CF, SP, and CM measurement, up to 25-fold

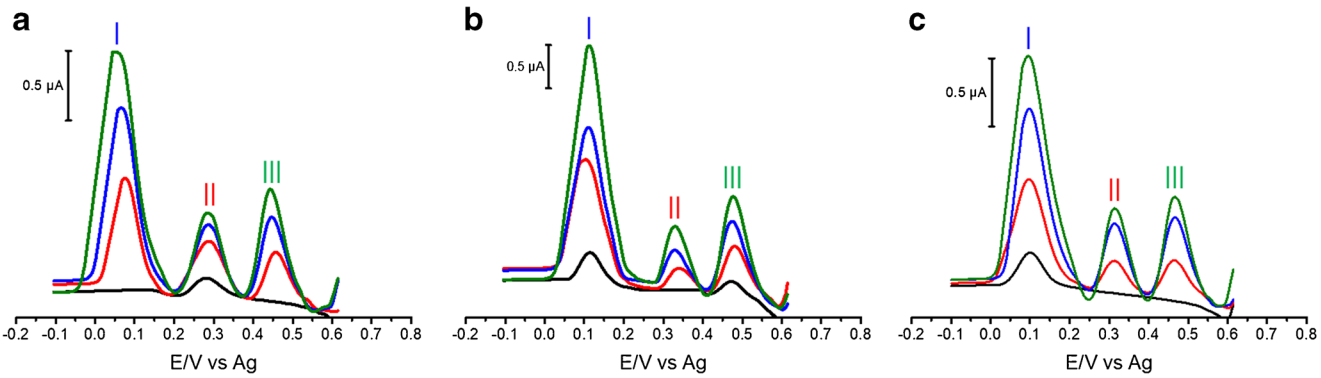

Fig. 5 Differential pulse voltammograms for sample analysis at SPE-CB-WS_2/AuNP-CT sensor. Class-selective hCN-based determination in food samples: rapeseed oil extract (**A**), *Kalanchoe crenata* (**B**), and apple juices (**C**); peak I (CF equivalents), peak II (SP equivalents), peak III (CM equivalents). Samples spiked with three increasing concentrations of the mixture of CF, SP, and CM (unspiked samples: black line). Spiked samples, CF, SP, and CM concentrations, respectively: 5, 10, and 15 μmol L^{-1} (red line); 10, 20, and 30 μmol L^{-1} (blue line); 15, 30, and 45 μmol L^{-1} (green line). Conditions: 0.1 mmol L^{-1} PB + 0.1 KCl, pH 7.0; pulse width 50 ms, modulation amplitude 50 mV, scan rate of 25 mV s^{-1}

Table 2 Determination of hCN equivalents in food samples

Sample[a]	Added (μmol L^{-1})			Found (μmol L^{-1})			Recovery (%)			RSD (%)		
	CF	SP	CM	CF	SP	CM	CF	SP	CM	CF	SP	CM
Rapeseed oil	-	-	-	3.3	6.3	<LOD	-	-	-	4	2	
	5	10	15	8.7	16.6	15.2	108	103	101	3	4	1
	10	20	30	14.1	24.5	32.5	108	91	109	1	3	3
	15	30	45	18.9	32.2	43.7	104	87	97	1	2	5
Kalanchoe crenata			-	5.3	<LOD	13.5		-	-	3	-	3
	5	10	15	10.0	10.4	29.4	94	104	106	4	4	3
	10	20	30	14.6	17.7	46.0	95	89	109	4	4	3
	15	30	45	18.6	29.6	59.0	86	99	101	1	3	2
Apple juice	-	-	-	3.5	<LOD	2.4	-	-	-	4	-	4
	5	10	15	8.6	9.3	16.0	102	93	91	2	3	4
	10	20	30	12.6	21.1	32.8	91	105	101	1	2	3
	15	30	45	16.9	27.8	42.3	89	93	87	1	4	4
Apple puree	-	-	-	8.2	<LOD	1.2	-	-	-	1	-	3
	5	10	15	13.1	8.7	15.4	98	87	94	1	3	4
	10	20	30	18.7	20.1	35.9	105	100	88	1	4	4
	15	30	45	24.2	26.0	42.4	109	87	94	1	4	3
Apple homogenized	-	-	-	5.3	<LOD	<LOD	-	-	-	2	-	-
	5	10	15	10.5	9.0	13.4	104	90	89	4	3	3
	10	20	30	14.2	17.3	27.3	90	87	88	2	4	4
	15	30	45	21.6	26.5	39.2	109	88	87	1	4	4

[a] Data expressed as mean value, $n = 3$

its average content in the studied samples. In conclusion, no interferences are found, indicating the selectivity for the simultaneous determination of hCN analogs.

Table 3 summarizes the main features of nanomaterial-based electrodes employed for direct (without accumulation step) simultaneous phenolic acid classes' determination.

Table 3 Nanomaterial-based electrodes for simultaneous phenolic acid classes' determination

Electrode/ manomaterial	Technique	Sample	Analyte	Linear range (μmol L^{-1})	LOD (μmol L^{-1})	Fouling resistance ($i_{p,a}$ decrease)	Ref.
CPE-$NiTiO_3$	DPV	Peeling skin lotion	o-Hydroxybenzoic acid, *p*-hydroxybenzoic acids	10–90, 10–90	0.38, 0.10	5%, $n = 15$	[38]
PTE-CB	DPV	Olive oil	Ortho-diphenols, monophenols	10–75, 10–75	6.0, 20.0	12%, $n = 26$	[35]
GCE-polyPCV/ f-SWCNTs	DPV	Cognac and brandy	Gallic acid, ellagic acids	0.75–10, 0.75–10	0.11, 0.12	-	[39]
GCE-rGO	SWV	Mango juice	Gallic acid, protocatechuic acids	20–144, 20–166	30.8, 10.2	5%, $n = 10$	[40]
SPE-CB-WS_2/ AuNP-CT	DPV	Rapeseed oil, *Kalanchoe crenata*, apple juice, apple puree, apple homogenized	Caffeic acid, sinapic acid, *p*-coumaric acid	0.4–112.5, 0.7–125.0, 1.4–93.7	0.09, 0.36, 0.39	3%, $n = 15$ (three analytes simultaneous determination)	This work

[a] *CPE-$NiTiO_3$*, carbon paste electrode modified with nickel titanate nanoceramic; *PTE-CB*, press-transferred carbon black electrode; *GCE-polyPCV/f-SWCNTs*, glassy carbon electrode modified with polyaminobenzene sulfonic acid–functionalized single-walled carbon nanotubes; *GCE-rGO*, glassy carbon electrode modified with reduced graphene oxide

The results obtained in the present study compared with other nanomaterial-based electrodes demonstrate better or comparable performances in terms of LOD, linear range, and reusability (in terms of fouling resistance). However, no works regarding the simultaneous detection and determination of CF, SP, and CM have been found, and most of them concern the simultaneous determination only of two phenolic acid classes. Noteworthy, little evidence is provided regarding the fouling resistance, which is the main limitation in electrochemical analysis of these compounds. In our opinion, the latter drawback is the main reason for the absence of electroanalytical approaches devoted to the simultaneous measurement of hCNs.

Definitely the "electrochemical approach" still remains attractive to study PCs' "antioxidant capacity." Indeed, conceptually speaking, the "electrochemical approach" can return qualitative and quantitative information regarding antioxidant capacity, since phenols' "oxidations" obtained at lowest potentials are inherently correlated with high antioxidant capacities [41, 42]. This valuable information is not obtainable with classic spectrophotometric methods. On the other hand, despite the chromatographic methods enable to assess polyphenols' composition and content, they are not able to evaluate the antioxidant capacity (neither total as well as of classes of compounds) [43]. Thus, in our opinion, taking advantage of a new generation of nanomaterials with amazing and under exploited *hidden* features, the electrochemical approach could result more and more competitive and spendable in lab and in field in the near future.

Conclusions

A high-performance electrochemical sensor based on WS_2 decorated with AuNP-CT and supported in a CB network was successfully developed and applied to the simultaneous determination of a three hCN-based polyphenolic class indexes (accordingly to the hydroxyl moieties' arrangement in the phenol structure) in food samples. The proposed sensor takes advantage of the AuNP-CT metallic properties, demonstrating electroactivity towards hydroxyl moieties through assembly in the WS_2 flakes that result in an enhanced conductivity with an exceptional antifouling activity due to WS_2. The final assembly of WS_2/AuNP-CT into CB network exhibited a further conductivity enhancement without loss of antifouling performance. The nanomaterial-based synergistic effect of the sensor results in enhanced selectivity, sensitivity, and reproducibility in the simultaneous determination of class-selective hCN structural analogs in food samples. Given its excellent electrochemical performance, together with its low cost, disposability, and ease of use, this SPE-CB-WS_2/AuNP-CT nanocomposite-based sensor represents a powerful candidate for the development of electrochemical devices for the determination of (bio)compounds with high passivation tendency.

Acknowledgments FDP acknowledges the Ministry of Education, University and Research (MIUR) and European Social Fund (ESF) for the PON R&I 2014-2020 program, action 1.2 "AIM: Attraction and International Mobility" (AIM1894039-3).

EF and GF kindly acknowledge partial financial support from Consorzio per lo Sviluppo dei Sistemi a Grande Interfase (CSGI).

DR acknowledges funding from the European Union's Horizon 2020 research and innovation program under the Marie Skłodowska-Curie grant agreement No. 713714, University of Teramo and Abruzzo region.

DC acknowledges the PRIN 2017 ACTUaL project of the Italian Ministry of Education, University and Research (MIUR) for funding.

AE acknowledges Spanish Ministry of Economy, Industry and Competitiveness (CTQ2017-86441-C2-1-R) and TRANSNANOAVANSENS program (S2018/NMT-4349) from the Community of Madrid.

Compliance with ethical standards

Conflict of interest The authors declare that they have no conflict of interest

References

1. El Gharras H (2009) Polyphenols: food sources, properties and applications - a review. Int J Food Sci Technol 44:2512–2518. https://doi.org/10.1111/j.1365-2621.2009.02077.x
2. Dela Pelle F, Compagnone D (2018) Nanomaterial-based sensing and biosensing of phenolic compounds and related antioxidant capacity in food. Sensors 18:462. https://doi.org/10.3390/s18020462
3. Del Rio D, Rodriguez-Mateos A, Spencer JPE et al (2013) Dietary (poly)phenolics in human health: structures, bioavailability, and evidence of protective effects against chronic diseases. Antioxid Redox Signal 18:1818–1892. https://doi.org/10.1089/ars.2012.4581
4. Serafini M, Peluso I (2016) Functional foods for health: the interrelated antioxidant and anti-inflammatory role of fruits, vegetables, herbs, spices and cocoa in humans. Curr Pharm Des 22:6701–6715. https://doi.org/10.2174/1381612823666161123094235
5. Teixeira J, Gaspar A, Garrido EM, Garrido J, Borges F (2013) Hydroxycinnamic acid antioxidants: an electrochemical overview. Biomed Res Int 2013:. https://doi.org/10.1155/2013/251754
6. Huang X, Zeng Z, Zhang H (2013) Metal dichalcogenide nanosheets: preparation, properties and applications. Chem Soc Rev 42:1934–1946. https://doi.org/10.1039/c2cs35387c
7. Pumera M, Loo AH (2014) Layered transition-metal dichalcogenides (MoS2and WS2) for sensing and biosensing. TrAC - Trends Anal Chem 61:49–53. https://doi.org/10.1016/j.trac.2014.05.009
8. Su S, Xu Y, Sun Q, Gu X, Weng L, Wang L (2018) Noble metal nanostructure-decorated molybdenum disulfide nanocomposites: synthesis and applications. J Mater Chem B 6:5323–5334. https://doi.org/10.1039/c8tb01659c
9. Della Pelle F, Daniel R, Scroccarello A et al (2019) High-performance carbon black/molybdenum disulfide nanohybrid sensor for cocoa catechins determination using an extraction-free approach. Sensors Actuators B Chem 296:126651. https://doi.org/10.1016/j.snb.2019.126651
10. Rojas D, Della Pelle F, Del Carlo M et al (2019) Nanohybrid carbon black-molybdenum disulfide transducers for preconcentration-free voltammetric detection of the olive oil o-diphenols hydroxytyrosol and oleuropein. Microchim Acta 186:363. https://doi.org/10.1007/s00604-019-3418-5

11. Aziz A, Asif M, Ashraf G, Azeem M, Majeed I, Ajmal M, Wang J, Liu H (2019) Advancements in electrochemical sensing of hydrogen peroxide, glucose and dopamine by using 2D nanoarchitectures of layered double hydroxides or metal dichalcogenides. A review Microchim Acta 186:671. https://doi.org/10.1007/s00604-019-3776-z
12. Polyakov AY, Yadgarov L, Popovitz-Biro R, Lebedev VA, Pinkas I, Rosentsveig R, Feldman Y, Goldt AE, Goodilin EA, Tenne R (2014) Decoration of ws2 nanotubes and fullerene-like mos2 with gold nanoparticles. J Phys Chem C 118:2161–2169. https://doi.org/10.1021/jp407388h
13. Dunklin JR, Lafargue P, Higgins TM, et al (2017) Production of monolayer-rich gold-decorated 2H–WS 2 nanosheets by defect engineering. npj 2D Mater Appl 1:43. https://doi.org/10.1038/s41699-017-0045-z
14. Wang Y, Ma J, Ye X, Wong WL, Li C, Wu K (2018) Enhanced effects of ionic liquid and gold nanoballs on the photoelectrochemical sensing performance of WS2 nanosheets towards 2,4,6-tribromophenol. Electrochim Acta 271:551–559. https://doi.org/10.1016/j.electacta.2018.03.176
15. Puangjan A, Chaiyasith S (2016) An efficient ZrO2/Co3O4/reduced graphene oxide nanocomposite electrochemical sensor for simultaneous determination of gallic acid, caffeic acid and protocatechuic acid natural antioxidants. Electrochim Acta 211:273–288. https://doi.org/10.1016/j.electacta.2016.04.185
16. Yola ML, Atar N (2014) A novel voltammetric sensor based on gold nanoparticles involved in p-aminothiophenol functionalized multi-walled carbon nanotubes: application to the simultaneous determination of quercetin and rutin. Electrochim Acta 119:24–31. https://doi.org/10.1016/j.electacta.2013.12.028
17. Elçin S, Yola ML, Eren T, Girgin B, Atar N (2016) Highly selective and sensitive voltammetric sensor based on ruthenium nanoparticle anchored calix[4]amidocrown-5 functionalized reduced graphene oxide: simultaneous determination of quercetin, morin and rutin in grape wine. Electroanalysis 28:611–619. https://doi.org/10.1002/elan.201500495
18. Rojas D, Pelle F, Carlo M et al (2020) Group VI transition metal dichalcogenides as antifouling transducers for electrochemical oxidation of catechol-containing structures. Electrochem Commun 106718:106718. https://doi.org/10.1016/j.elecom.2020.106718
19. Della Pelle F, Vilela D, González MC, Lo Sterzo C, Compagnone D, del Carlo M, Escarpa A (2015) Antioxidant capacity index based on gold nanoparticles formation. Application to extra virgin olive oil samples. Food Chem 178:70–75. https://doi.org/10.1016/j.foodchem.2015.01.045
20. Della Pelle F, Scroccarello A, Sergi M, Mascini M, del Carlo M, Compagnone D (2018) Simple and rapid silver nanoparticles based antioxidant capacity assays: reactivity study for phenolic compounds. Food Chem 256:342–349. https://doi.org/10.1016/j.foodchem.2018.02.141
21. Della Pelle F, Angelini C, Sergi M, del Carlo M, Pepe A, Compagnone D (2018) Nano carbon black-based screen printed sensor for carbofuran, isoprocarb, carbaryl and fenobucarb detection: application to grain samples. Talanta 186:389–396. https://doi.org/10.1016/j.talanta.2018.04.082
22. Pirisi FM, Cabras P, Cao CF, Migliorini M, Muggelli M (2000) Phenolic compounds in virgin olive oil. 2. Reappraisal of the extraction, HPLC separation, and quantification procedures. J Agric Food Chem 48:1191–1196
23. Rothwell JA, Perez-Jimenez J, Neveu V, et al (2013) Phenol-Explorer 3.0: a major update of the Phenol-Explorer database to incorporate data on the effects of food processing on polyphenol content. Database. https://doi.org/10.1093/database/bat070
24. Shi Y, Huang JK, Jin L, Hsu YT, Yu SF, Li LJ, Yang HY (2013) Selective decoration of Au nanoparticles on monolayer MoS2 single crystals. Sci Rep 3:1839. https://doi.org/10.1038/srep01839
25. Gan X, Zhao H, Quan X, Zhang Y (2016) An electrochemical sensor based on p-aminothiophenol/Au nanoparticle-decorated HxTiS2 nanosheets for specific detection of picomolar Cu (II). Elsevier Ltd
26. Della Pelle F, González MC, Sergi M, del Carlo M, Compagnone D, Escarpa A (2015) Gold nanoparticles-based extraction-free colorimetric assay in organic media: an optical index for determination of total polyphenols in fat-rich samples. Anal Chem 87:6905–6911. https://doi.org/10.1021/acs.analchem.5b01489
27. Scroccarello A, Della Pelle F, Fratini E, Ferraro G, Scarano S, Palladino P, Compagnone D (2020) Colorimetric determination of polyphenols via gold nanoseeds decorated polydopamine film. Microchim Acta 187:267. https://doi.org/10.1007/s00604-020-04228-4
28. Choi Y, Choi MJ, Cha SH, Kim Y, Cho S, Park Y (2014) Catechin-capped gold nanoparticles: green synthesis, characterization, and catalytic activity toward 4-nitrophenol reduction. Nanoscale Res Lett 9:1–8. https://doi.org/10.1186/1556-276X-9-103
29. Zhang C, Hu DF, Xu JW, Ma MQ, Xing H, Yao K, Ji J, Xu ZK (2018) Polyphenol-assisted exfoliation of transition metal dichalcogenides into nanosheets as photothermal nanocarriers for enhanced antibiofilm activity. ACS Nano 12:12347–12356. https://doi.org/10.1021/acsnano.8b06321
30. Nicholson RS (1965) Theory and application of cyclic voltammetry for measurement of electrode reaction kinetics. Anal Chem 37:1351–1355
31. Lavagnini I, Antiochia R, Magno F (2004) An extended method for the practical evaluation of the standard rate constant from cyclic voltammetric data. Electroanalysis 16:505–506. https://doi.org/10.1002/elan.200302851
32. Della Pelle F, Del Carlo M, Sergi M et al (2016) Press-transferred carbon black nanoparticles on board of microfluidic chips for rapid and sensitive amperometric determination of phenyl carbamate pesticides in environmental samples. Microchim Acta 183:3143–3149. https://doi.org/10.1007/s00604-016-1964-7
33. Mazzaracchio V, Tomei MR, Cacciotti I, Chiodoni A, Novara C, Castellino M, Scordo G, Amine A, Moscone D, Arduini F (2019) Inside the different types of carbon black as nanomodifiers for screen-printed electrodes. Electrochim Acta 317:673–683. https://doi.org/10.1016/j.electacta.2019.05.117
34. Della Pelle F, Vázquez L, Del Carlo M et al (2016) Press-printed conductive carbon black nanoparticle films for molecular detection at the microscale. Chem - A Eur J 22:12761–12766. https://doi.org/10.1002/chem.201601743
35. Della Pelle F, Di Battista R, Vázquez L et al (2017) Press-transferred carbon black nanoparticles for class-selective antioxidant electrochemical detection. Appl Mater Today 9:29–36. https://doi.org/10.1016/j.apmt.2017.04.012
36. Scroccarello A, Della Pelle F, Neri L, Pittia P, Compagnone D (2019) Silver and gold nanoparticles based colorimetric assays for the determination of sugars and polyphenols in apples. Food Res Int 119:359–368. https://doi.org/10.1016/j.foodres.2019.02.006
37. Della Pelle F, Scroccarello A, Scarano S, Compagnone D (2019) Silver nanoparticles-based plasmonic assay for the determination of sugar content in food matrices. Anal Chim Acta 1051:129–137. https://doi.org/10.1016/j.aca.2018.11.015
38. Kashani FZ, Ghoreishi SM, Khoobi A, Enhessari M (2019) A carbon paste electrode modified with a nickel titanate nanoceramic for simultaneous voltammetric determination of ortho- and para-hydroxybenzoic acids. Microchim Acta 186:2–9. https://doi.org/10.1007/s00604-018-3113-y
39. Ziyatdinova G, Guss E, Morozova E, Budnikov H, Davletshin R, Vorobev V, Osin Y (2019) Simultaneous voltammetric determination of gallic and ellagic acids in cognac and brandy using electrode modified with functionalized SWNT and poly(pyrocatechol violet).

Food Anal Methods 12:2250–2261. https://doi.org/10.1007/s12161-019-01585-6

40. Abdel-Hamid R, Bakr A, Newair EF, Garcia F (2019) Simultaneous voltammetric determination of gallic and protocatechuic acids in mango juice using a reduced graphene oxide-based electrochemical sensor. Beverages 5:17. https://doi.org/10.3390/beverages5010017
41. Blasco AJ, González MC, Escarpa A (2004) Electrochemical approach for discriminating and measuring predominant flavonoids and phenolic acids using differential pulse voltammetry: towards an electrochemical index of natural antioxidants. Anal Chim Acta 511:71–81. https://doi.org/10.1016/j.aca.2004.01.038
42. Blasco AJ, Rogerio MC, González MC, Escarpa A (2005) "Electrochemical index" as a screening method to determine "total polyphenolics" in foods: a proposal. Anal Chim Acta 539:237–244. https://doi.org/10.1016/j.aca.2005.02.056
43. Escarpa A, González MC (2001) Approach to the content of total extractable phenolic compounds from different food samples by comparison of chromatographic and spectrophotometric methods. Anal Chim Acta 427:119–127. https://doi.org/10.1016/S0003-2670(00)01188-0